EPJ AP

Applied Physics

EPJ.org

your physics journal

Eur. Phys. J. Appl. Phys. (2015) 71: 20807 DOI: 10.1051/epjap/2015140515

Density distributions of OH, Na, water vapor, and water mist in atmospheric-pressure dc helium glow plasmas in contact with NaCl solution

Koichi Sasaki, Hiroaki Ishigame, and Shusuke Nishiyama

edp sciences

The title “The European Physical Journal” is a joint property of EDP Sciences, Società Italiana di Fisica (SIF) and Springer

Eur. Phys. J. Appl. Phys. (2015) 71: 20807
DOI: 10.1051/epjap/2015140515

THE EUROPEAN PHYSICAL JOURNAL APPLIED PHYSICS

Regular Article

Density distributions of OH, Na, water vapor, and water mist in atmospheric-pressure dc helium glow plasmas in contact with NaCl solution*

Koichi Sasaki[a], Hiroaki Ishigame, and Shusuke Nishiyama

Division of Quantum Science and Engineering, Hokkaido University, Kita 13, Nishi 8, Kita-ku, Sapporo 060-8628, Japan

Received: 29 December 2014 / Received in final form: 28 February 2015 / Accepted: 10 March 2015
Published online: 15 July 2015 –

Abstract. This paper reports the density distributions of OH, Na, water vapor and water mist in atmospheric-pressure dc helium glow plasmas in contact with NaCl solution. The densities of OH, Na and H_2O had different spatial distributions, while the Na density had a similar distribution to mist, suggesting that mist is the source of Na in the gas phase. When the flow rate of helium toward the electrolyte surface was increased, the distributions of all the species densities concentrated in the neighboring region to the electrolyte surface more significantly. The densities of all the species were sensitive to the electric polarity of the power supply. In particular, we never detected Na and mist when the electrolyte worked as the anode of the dc discharge.

1 Introduction

Plasma-liquid interaction is a new subject in the field of reactive plasmas. The attention focused on the plasma-liquid interaction is driven by its importance in practical applications, such as the treatment of liquid media including sterilization [1–4], the treatment of biological tissues and plasma medicine [5,6]. The research of plasma-surface interaction has a long history, but almost all the works to date examined the interaction between plasmas and solid surfaces. Although solids and liquids have common nature as condensed matters, the plasma-liquid interaction includes processes different from those of the plasma-solid interaction such as evaporation and mist formation. We believe that plasma-liquid interaction is a tough subject, and intensive investigations are necessary to accumulate comparable knowledge to plasma-solid interaction.

A driving force for the research of plasma-liquid interaction is the development of various methods for producing atmospheric-pressure plasmas. Among various methods for producing atmospheric-pressure plasmas in contact with liquids [7–18], in this work, we have employed dc glow discharge between a nozzle electrode and an electrolyte, which has been reported by Shirai and coworkers [19–22]. A reason for choosing this plasma source is that it can produce a stable positive column with a cathode sheath [23]. The structure of the positive column is similar to conventional one produced in a gas at a reduced pressure; hence this plasma source is suitable for the fundamental investigation on the plasma-liquid interaction.

In this work, we examined the density distributions of OH, Na, water vapor and water mist, in the helium glow plasma in contact with an electrolyte (1% NaCl solution). Laser-induced fluorescence (LIF) spectroscopy was adopted for measuring the density distributions of OH and Na. The density distribution of water vapor was estimated from the distribution of the collisional quenching frequency of OH($A^2\Sigma^+$). The distribution of mist was examined by laser Mie scattering. Although the diagnostics were limited in the gas-phase side of the plasma-liquid interface, the experimental results give us insight into plasma-liquid interaction.

2 Experiment

The experimental apparatus is schematically shown in Figure 1. The plasma source used in this work was identical to that reported by Shirai and coworkers [19–23]. A dc power supply was connected between a stainless-steel gas nozzle and a platinum wire via a resister of 100 kΩ. In this paper, we examined the influence of the electric polarity of the dc power supply on the densities of OH, Na, H_2O, and mist. The platinum wire was immersed in 1% NaCl solution which filled a square acrylic vessel with quartz windows. The inner and outer diameters of the nozzle electrode were 0.48 and 0.70 mm, respectively, and the distance between the top of the nozzle electrode and the surface of the NaCl solution was 4 mm. Helium as a working gas was fed from the nozzle toward the electrolyte

[a] e-mail: sasaki@qe.eng.hokudai.ac.jp

* Contribution to the topical issue "The 14th International Symposium on High Pressure Low Temperature Plasma Chemistry (HAKONE XIV)", edited by Nicolas Gherardi, Ronny Brandenburg and Lars Stollenwark

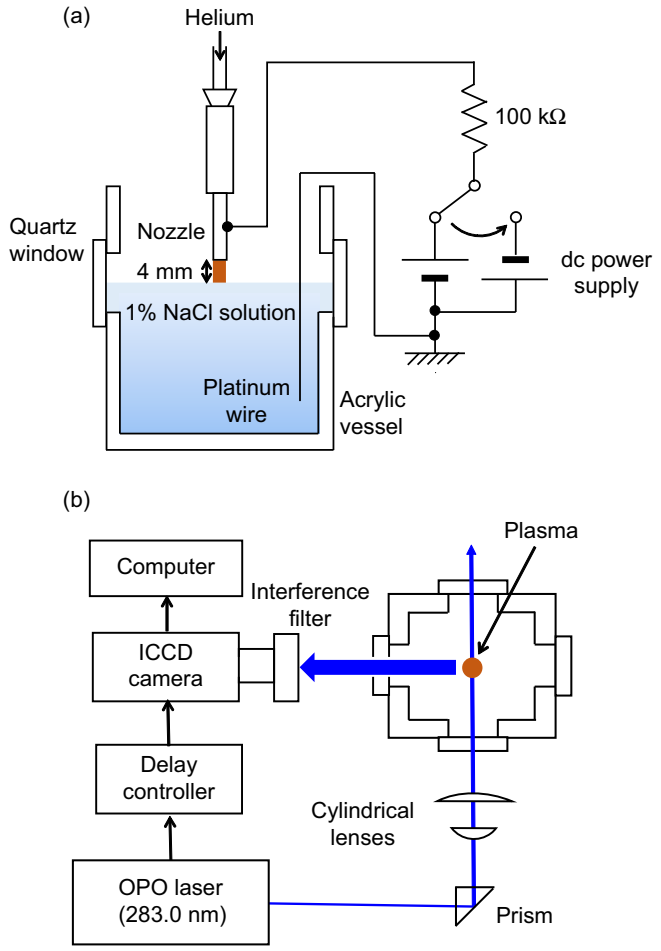

Fig. 1. Experimental apparatus. (a) Side view showing the plasma source and (b) top view showing the apparatus of LIF imaging spectroscopy.

surface. The gas flow rate was controlled using a mass flow controller.

We adopted LIF imaging spectroscopy to measure the spatial distributions of OH and Na densities in the discharge space. In the LIF measurement, OH or Na at the electronic ground state is transferred to an excited state by absorbing laser photons at the resonant wavelength with the transition line. The LIF intensity, which is obtained by the radiative decay of the excited state, is proportional to the density of OH or Na at the ground state such that:

$$I_{\mathrm{LIF}} \propto An_2 \propto n_1, \tag{1}$$

where n_1 and n_2 are the densities of the ground and laser-excited states, respectively, and A is the transition probability of the LIF line. In general, the absolute calibration of the ground-state density is possible with the help of absorption spectroscopy, but we did not determine the absolute OH and Na densities in this work.

As shown in Figure 1b, the tunable laser beam yielded from an optical parametric oscillator (OPO) was injected into the $r-z$ plane of the cylindrically symmetric discharge space after arranging its shape to be planar using two cylindrical lenses. The thickness of the planar laser beam was 1 mm, while the width of the planar laser beam was slightly larger than 4 mm. The LIF formed an image on the planar laser beam. The LIF image was captured using a charge-coupled device camera with a gated image intensifier (ICCD camera) from the angle normal to the incident laser beam. An interference filter was placed in front of the camera to discriminate LIF from the self-emission of the plasma.

The wavelength of the OPO laser for obtaining LIF of OH was approximately 283.0 nm, which excited OH at $X^2\Pi(v''=0)$ to $A^2\Sigma^+(v'=1)$. The fluorescence was obtained at the two transitions of $A^2\Sigma^+(v'=1) \rightarrow X^2\Pi(v''=1)$ and $A^2\Sigma^+(v'=0) \rightarrow X^2\Pi(v''=0)$. The latter LIF was caused by the vibrational energy transfer from laser-excited $A^2\Sigma^+(v'=1)$ to $A^2\Sigma^+(v'=0)$ [24]. The transition line of LIF for Na was the D line at the wavelength of 589.00 nm ($^2S_{1/2} - {}^2P^{\mathrm{o}}_{3/2}$). Although the wavelengths of the excitation and the fluorescence were the same in the LIF measurement of the Na density, the signal to noise (the stray light) ratio was much higher than unity in the present experiment.

We carefully examined the influences of collisional quenching and rotational temperature in the LIF measurement of the OH density in a previous paper [25]. The principal quencher of laser-excited OH($A^2\Sigma^+$) was water vapor (H_2O) in this experimental condition, and the spatial distribution of the H_2O density was estimated by examining the spatial distribution of the quenching frequency. The spatial distribution of the quenching frequency was obtained by capturing the LIF images at various delay times after the injection of the tunable laser pulse. The collisional quenching frequency of laser-excited Na($^2P^{\mathrm{o}}$) was also examined in the present work using the same manner as that in the previous work for OH radicals [25]. The rotational temperature of OH($X^2\Pi$ ($v''=0$)) was evaluated by measuring the LIF intensities which were obtained at the laser wavelengths corresponding to the Q branch excitations from rotational states with rotational quantum numbers of $J''=4$, 6, 7, 9 and 10. The spatial distribution of the rotational temperature was obtained from the relationship between the LIF intensity and the energy of the rotational state (the Boltzmann plot) at each pixel of the ICCD camera.

In addition to the density distributions of OH, Na and H_2O, we examined the spatial distribution of water mist in the present work. Since mist is a kind of particulate, we adopted laser Mie scattering for detecting it. The OPO laser in Figure 1b was replaced with the second harmonic of a Nd:YAG laser. The image of the scattered laser light was captured using the same ICCD camera as that used in the LIF measurement. An interference filter at the same wavelength as the incident laser beam was placed in front of the ICCD camera.

3 Results

Figure 2 shows the distribution of the OH density, which was observed at a gas flow rate of 73 ccm. The discharge voltage and the discharge current were 950 V and 40 mA, respectively. The positions of the nozzle electrode and the electrolyte (NaCl solution) are illustrated in the figure.

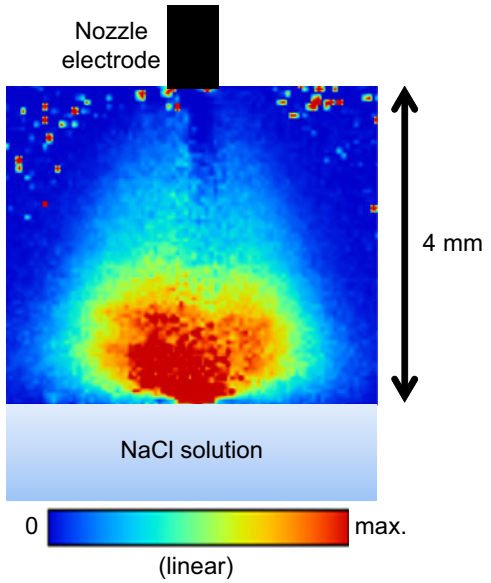

Fig. 2. Distribution of OH density observed at a gas flow rate of 73 ccm. The discharge current and the discharge voltage were 40 mA and 950 V, respectively. The nozzle electrode works as the anode of the discharge.

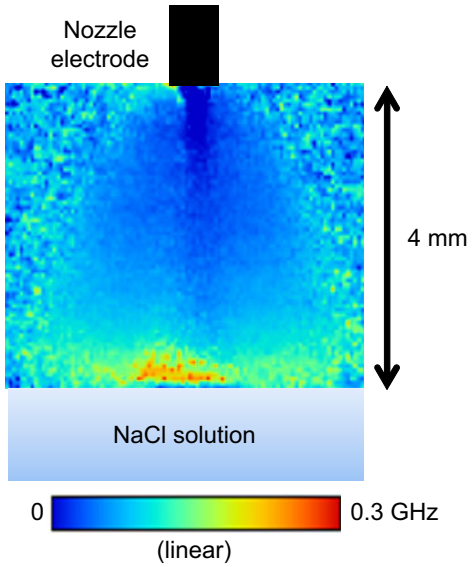

Fig. 3. Distribution of the frequency of collisional quenching for OH($A^2\Sigma^+$). The discharge parameters are the same as those in Figure 2. This figure roughly represents the distribution of the H_2O density.

The nozzle electrode and the platinum wire were connected to the positive and negative sides of the dc power supply, respectively. The distribution shown in Figure 2 was reconstructed from the LIF image by considering the spatial distributions of the quenching frequency of the laser-excited OH($A^2\Sigma^+$) and the rotational temperature of OH($X^2\Pi$). The detailed procedure for obtaining the spatial distribution of the OH density has been described in the previous paper [25].

The spatial distribution of the collisional quenching frequency of laser-excited OH($A^2\Sigma^+$) is shown in Figure 3. The gas flow rate, the discharge voltage, the discharge current and the electric polarity of the dc power supply were the same as those in Figure 2. As described in the previous paper [25], H_2O has the highest frequency of collisional quenching for OH($A^2\Sigma^+$) among H_2O, N_2, O_2 and He [26–28]. Therefore, the distribution of the quenching frequency shown in Figure 3 roughly represents the distribution of the H_2O density, especially in the bottom part of the discharge space. According to the rate coefficient of collisional quenching of OH($A^2\Sigma^+$) by H_2O (7.23×10^{-10} cm^3/s) [26–28], the maximum H_2O density in the discharge space was estimated to be 4×10^{17} cm^{-3}.

Figure 4 shows the spatial distributions of the Na density and the collisional quenching frequency of laser-excited Na($^2P^o$). The gas flow rate, the discharge voltage, the discharge current and the electric polarity of the dc power supply were the same as those in Figure 2. The spatial distribution of the Na density shown in Figure 4a was reconstructed from the LIF image and the spatial distribution of the quenching frequency shown in Figure 4b. It is easily noticeable that the spatial distribution of the quenching frequency of Na($^2P^o$) is different from that of OH($A^2\Sigma^+$). According to the distribution shown in Figure 4b, it is speculated that ambient air (N_2 and O_2) largely contribute to collisional quenching of Na($^2P^o$).

The result of the mist detection in the discharge space is shown in Figure 5. The gas flow rate, the discharge voltage, the discharge current, and the electric polarity of the dc power supply were the same as those in Figure 2 The spots in the figure shows the scattered YAG laser light, which indicates the locations of mist. This is an experimental evidence of the mist production from the electrolyte irradiated by a plasma.

In this work, we examined the influence of the discharge conditions on the spatial distributions of the densities of OH, Na, H_2O and mist. A discharge parameter was the gas flow rate. Figure 6 shows the LIF images of OH, the spatial distributions of the collisional quenching frequencies of OH($A^2\Sigma^+$), the Na densities, and the images of laser Mie scattering, which were observed at gas flow rates of 73 and 219 ccm. The discharge current was fixed at 40 mA, and the discharge voltage was roughly unaffected by the gas flow rate. The influence of the spatial distribution of the collisional quenching frequency is compensated in the LIF images of OH, but the influence of the spatial distribution of the rotational temperature is not considered since the evaluation of the rotational temperature is seriously time consuming. Hence the LIF images shown in Figures 6a and 6b do not represent the real distributions of the OH densities; however we can roughly know how the gas flow rate affects the OH density. As shown in Figures 6a and 6b, the OH density decreased with the gas flow rate especially in the upstream region. The region with a high quenching frequency concentrated in the neighboring region to the electrolyte surface more significantly at a higher flow rate, as shown in Figures 6c and 6d. Note that the experimental result shown in Figure 6c

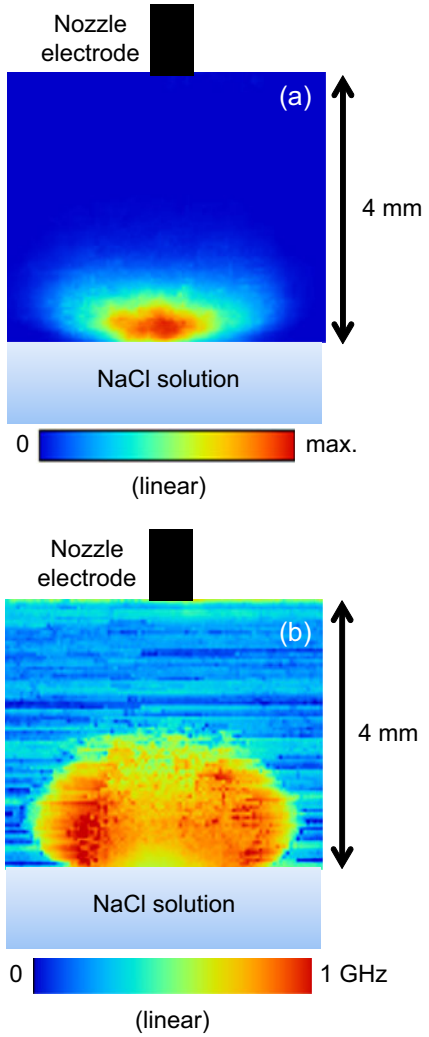

Fig. 4. LIF results for Na at the same discharge parameters as those in Figure 2. (a) Distribution of Na density and (b) distribution of quenching frequency of laser-produced Na($^2P^o$).

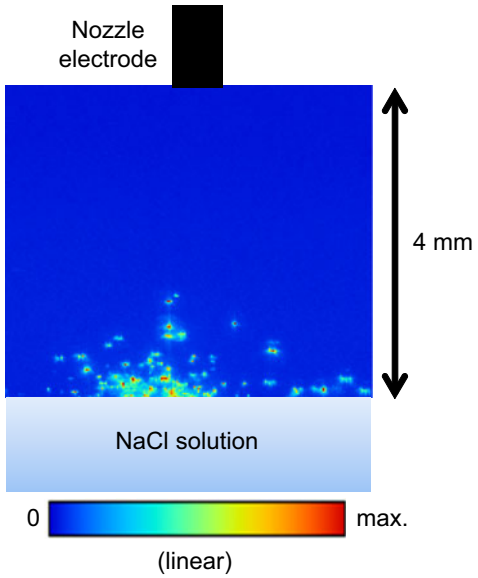

Fig. 5. Distribution of mist in the discharge space, which was examined by laser Mie scattering. The discharge parameters are the same as those in Figure 2.

is different from Figure 3, even though they were obtained at the same discharge condition. Although the discharge condition was the same, the experiments shown in Figures 3 and 6c were carried out on different days in winter and summer, respectively, suggesting that the H_2O density was affected by the humidity in the laboratory. The Na density also decreased with the gas flow rate as shown in Figures 6e and 6f. The distribution of the Na density concentrated in the neighboring region to the electrolyte surface more significantly at a higher gas flow rate. This was also the case for mist. As shown in Figures 6g and 6h, the concentrated distribution of mist was observed at a high gas flow rate.

Another discharge parameter was the electric polarity of the dc power supply. The experimental results shown in Figures 2–6 were obtained when the electrolyte worked as the cathode of the dc discharge. Figure 7 shows the influence of the polarity of the power supply on the LIF image of OH and the distribution of the collisional quenching frequency of OH($A^2\Sigma^+$). The discharge current and the gas flow rates were fixed at 30 mA and 73 ccm, respectively. The discharge voltage was 940 V when the electrolyte worked as the cathode, while it was 800 V when the electrolyte worked as the anode of the discharge. Only the influence of collisional quenching was compensated in the LIF images of OH. As shown in the figure, we observed lower densities of OH and H_2O when the electrolyte worked as the anode of the discharge. In addition, it should be emphasized that we never detected Na and mist in the discharge space, when the electrolyte worked as the anode of the discharge.

4 Discussion

In the previous paper [25], we discussed the production, the transport, and the loss processes of OH radicals in the plasma in contact with the 1% NaCl solution on the basis of the density distribution shown in Figure 2. The peak position of the OH density shown in Figure 2 was located in the region close to the electrolyte, but it was surely separated from its surface. In addition, the OH density on the electrolyte surface was not zero. From these results, we can say that OH radicals are produced in the gas-phase of the plasma, and they are transported back toward the electrolyte surface. The electrolyte surface interacts with OH radicals as their sink. A possibility of the loss process on the electrolyte surface is recombination to form H_2O_2 and H_2O. In addition, we can expect the transport of OH radicals into the inside of the electrolyte. In contrast to the OH density, the peak position of the quenching frequency is in contact with the electrolyte surface, as shown in Figure 3. This is reasonable since the major source of H_2O is the electrolyte in this experimental condition. Since H_2O is the parent of OH, the broader distribution of the

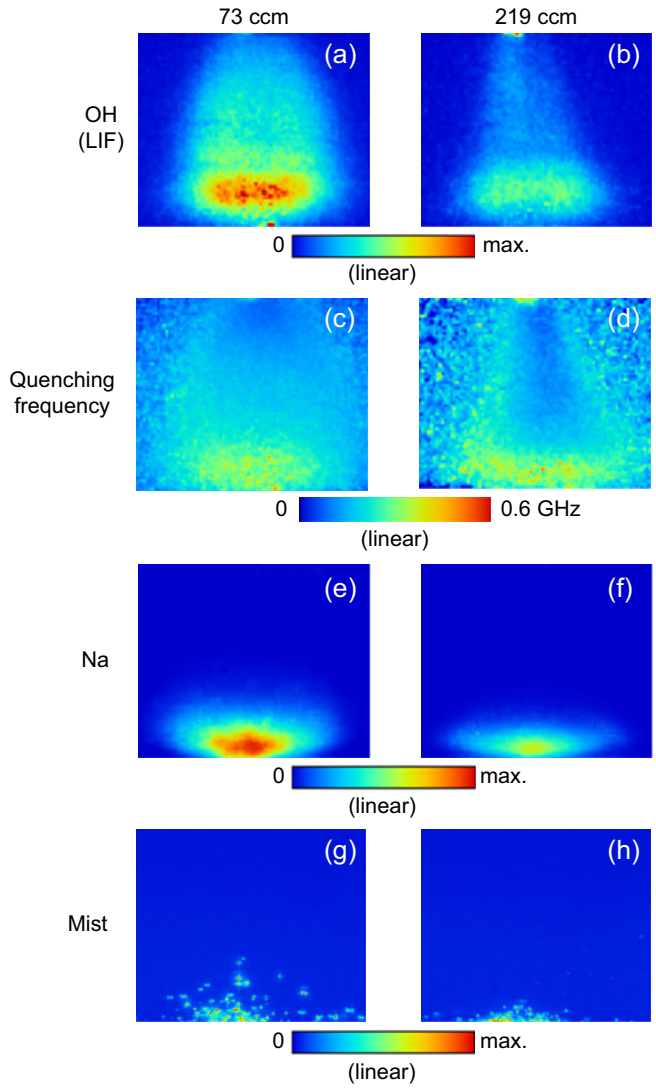

Fig. 6. Comparisons of the LIF images of OH ((a) and (b)), the spatial distributions of the collisional quenching frequency of OH($A^2\Sigma^+$) ((c) and (d)), the Na densities ((e) and (f)), and the images of laser Mie scattering ((g) and (h)) observed at gas flow rates of 73 and 219 ccm. The discharge current was fixed at 40 mA.

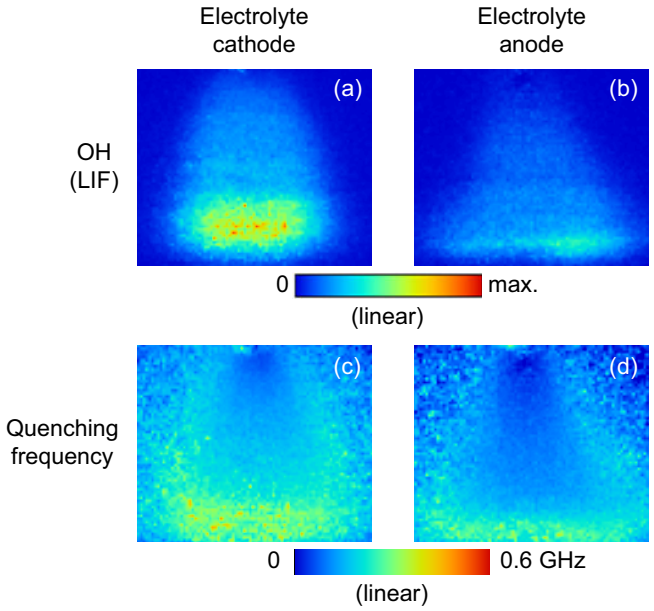

Fig. 7. Comparisons of the LIF images of OH ((a) and (b)) and the spatial distributions of the collisional quenching frequency of OH($A^2\Sigma^+$) ((c) and (d)), observed when the electrolyte worked as the cathode and the anode.

OH density than the quenching frequency indicates the considerable transport of OH radicals. OH radicals originated from H_2O in ambient air partly contribute to the distribution of the OH density, since the OH density is affected by the humidity in the laboratory as shown in Figures 3 and 6c.

The peak position of the Na density shown in Figure 4a is separated from the electrolyte surface. This indicates that the source of Na is not the surface of the electrolyte but is in the gas phase of the plasma. A possible explanation for the negligible production of Na from the electrolyte surface is the repulsion of Na^+ in water by the electrostatic force, since the electrolyte worked as the cathode of the discharge in Figure 4. However, we observed a much lower (negligible) Na density when the electrolyte worked as the anode, indicating that the reduction of Na^+ at the plasma-liquid interface is negligible. This may be reasonable from the viewpoint of conventional electrolysis, where the product from the cathode electrode is not Na but is H_2.

On the other hand, the similar distributions of the Na density shown in Figure 4a and mist shown in Figure 5 suggest that mist in the gas phase is the source of Na. As has been reported in the previous paper [25], the gas temperature in the plasma is higher than 2000 K. Therefore, we can expect the vaporization of mist in the gas phase, resulting in the production of Na. Since the transport of Na is not expected because of the high reactivity, the Na density has the similar distribution to the mist density.

The experimental result shown in Figure 7 indicates the importance of power deposition onto the electrolyte on the production of water vapor and OH radicals. Although there was a difference of ∼15% in the discharge power when the electrolyte worked as the cathode and the anode, the differences in the OH density and the quenching frequency were greater than the power difference. This is because the dominant energy transport from the positive column is toward the cathode. The power deposition onto the electrolyte is especially important in the production of mist, since we never detected mist and Na in the discharge space when the electrolyte worked as the anode of the discharge. Minagawa and coworkers pointed out the importance of bombarding ion energy for the production of water vapor and water clusters by a molecular dynamic simulation [29]. They also pointed out the enhancement of cluster formation in the presence of intense electric field. The present experimental results agree with their molecular dynamic simulation qualitatively.

The experimental results observed at a higher gas flow rate (Fig. 6) indicates the importance of transport along the gas flow. The comparison between Figures 6a and 6b reveal that the upward transport of OH radicals is disturbed by the downward flow of He. In addition, as shown in Figures 6c–6h, the products from the electrolyte were pushed back toward the electrolyte surface. The experimental results indicate that the design of the gas flow is essentially important in the applications of plasma-liquid interaction such as plasma medicine. Further investigations on the plasma parameters, the gas (rotational) temperature, and the profile of the He flow are necessary to obtain better understanding on the influence of the gas flow rate on the structure of the discharge.

5 Conclusions

In this work, we examined the density distributions of OH, Na, water vapor and water mist in atmospheric-pressure dc helium glow plasmas in contact with NaCl solution. The experimental results indicate that OH and Na are produced in the gas-phase of the plasma. The parent molecule of OH is H_2O which is produced from the electrolyte. The source of Na is mist which is also produced from the electrolyte. The distributions of the densities of OH and Na indicates their transports toward the electrolyte surface. The power deposition is essentially important for the production of water vapor and water mist from the electrolyte. In addition, the gas flow affects significantly to the density distributions of all the species. This paper gives insight into plasma-liquid interaction, but further investigations are necessary to obtain advanced understanding on it.

The authors would like to thank Fumiyoshi Tochikubo and Naoki Shirai for the detailed information about the apparatus of the dc glow discharge plasma source.

References

1. B.R. Locke, M. Sato, P. Sunka, M.R. Hoffmann, J.S. Chang, Ind. Eng. Chem. Res. **45**, 882 (2006)
2. B. Sun, M. Sato, A. Harano, J.S. Clements, J. Electrostat. **43**, 115 (1998)
3. M. Laroussi, IEEE Trans. Plasma Sci. **24**, 1188 (1996)
4. S. Ikawa, K. Kitano, S. Hamaguchi, Plasma Processes Polym. **7**, 33 (2010)
5. G. Fridman, G. Friedman, A. Gutsol, A.B. Shekhter, V.N. Vasilets, A. Fridman, Plasma Processes Polym. **5**, 503 (2008)
6. M.G. Kong, G. Kroesen, G. Morfill, T. Nosenko, T. Shimizu, J. van Dijk, J.L. Zimmermann, New J. Phys. **11**, 115012 (2009)
7. P. Bruggeman, C. Leys, J. Phys. D **42**, 053001 (2009)
8. K. Sato, K. Yasuoka, IEEE Trans. Plasma Sci. **36**, 1144 (2008)
9. P. Bruggeman, J. Degroote, J. Vierendeels, C. Leys, Plasma Source. Sci. Technol. **17**, 025008 (2008)
10. T. Ishijima, H. Hotta, H. Sugai, Appl. Phys. Lett. **91**, 121501 (2007)
11. T. Ishijima, H. Sugiura, R. Saito, H. Toyoda, H. Sugai, Plasma Source. Sci. Technol. **19**, 015010 (2010)
12. T. Shirafuji, Y. Himeno, Jpn J. Appl. Phys. **52**, 11NE03 (2013)
13. M. Teschke, J. Kedzierski, E.G. Finatu-Dinu, D. Korzec, J. Engemann, IEEE Trans. Plasma Sci. **33**, 310 (2005)
14. V. Schulz-von der Gathen, L. Schaper, N. Knake, S. Reuter, K. Niemi, T. Gans, J. Winter, J. Phys. D **41**, 194004 (2008)
15. K. Urabe, T. Morita, K. Tachibana, B.N. Ganguly, J. Phys. D **43**, 095201 (2010)
16. F. Jia, N. Sumi, K. Ishikawa, H. Kano, H. Inui, J. Kularatne, K. Takeda, H. Kondo, M. Sekine, A. Kono, M. Hori, Appl. Phys. Expr. **4**, 026101 (2011)
17. D. Hayashi, W.F.L.M. Hoeben, G. Dooms, E.M. van Veldhuizen, W.R. Rutgers, G.M.W. Kroesen, J. Phys. D **33**, 2769 (2000)
18. P. Bruggeman, J. van Slycken, J. Degroote, J. Vierendeels, P. Verleysen, C. Leys, IEEE Trans. Plasma Sci. **36**, 1138 (2008)
19. N. Shirai, M. Nakazawa, S. Ibuka, S. Ishii, IEEE Trans. Plasma Sci. **36**, 1160 (2008)
20. N. Shirai, M. Nakazawa, S. Ibuka, S. Ishii, Jpn J. Appl. Phys. **48**, 036002 (2009)
21. N. Shirai, S. Ibuka, S. Ishii, Appl. Phys. Expr. **2**, 036001 (2009)
22. N. Shirai, K. Ichinose, S. Uchida, F. Tochikubo, Plasma Source. Sci. Technol. **20**, 034013 (2011)
23. F. Tochikubo, N. Shirai, S. Uchida, Appl. Phys. Expr. **4**, 056001 (2011)
24. S. Yonemori, Y. Nakagawa, R. Ono, T. Oda, J. Phys. D **45**, 225202 (2012)
25. H. Ishigame, S. Nishiyama, K. Sasaki, Jpn J. Appl. Phys. **54**, 01AF02 (2015)
26. U. Rahmann, W. Kreutner, K. Kohse-Höinghaus, Appl. Phys. B **69**, 61 (1999)
27. L.R. Williams, D.R. Crosley, J. Chem. Phys. **104**, 6507 (1996)
28. M. Tamura, P.A. Berg, J.E. Harrington, J. Luque, J.B. Jeffries, G.P. Smith, D.R. Crosley, Combust. Flame **114**, 502 (1998)
29. Y. Minagawa, N. Shirai, S. Uchida, F. Tochikubo, Jpn J. Appl. Phys. **53**, 010210 (2014)